RSC Advances

ROYAL SOCIETY OF CHEMISTRY

www.rsc.org/advances

Novel 3-D nanoporous graphitic-C_3N_4 nanosheets with heterostructured modification for efficient visible-light photocatalytic hydrogen production

Jielin Yuan,[a] Qiongzhi Gao,*[a] Xin Li,[a] Yingju Liu,[a] Yueping Fang, *[a] Siyuan Yang [c], Feng Peng [c] and Xiaosong Zhou*[b]

[a]*Institute of Biomaterial, College of Science, South China Agricultural University, Guangzhou 510642,China;*

[b]*School of Chemistry Science & Technology, and Institute of Physical Chemistry, Zhanjiang Normal University, Zhanjiang 524048,, China;*

[c] *School of Chemistry and Chemical Engineering, South China University of Technology, Guangzhou, PR China.*

Corresponence author: Y.P. Fang Tel: 86-20-85285565. Fax: 86-20-85285565. E-mail: ypfang@scau.edu.cn; X.S. Zhou E-mail: zxs801213@163.com

Abstract: Phosphorus-doped g-C_3N_4 (P-C_3N_4) nanosheets with unique 3-D nanoporous structures are synthesized by the first time in this work, such functional porous architectures coupled with $BiPO_4$ nanorods can exhibit superior photocatalytic activity for hydrogen production. X-ray diffraction (XRD), transmission electron microscopy (TEM), scanning electron microscope (SEM), X-ray photoelectron spectra (XPS) and UV-vis diffusive reflectance spectra have been employed to characterize the heterostructured photocatalytic materials. The as-prepared composite photocatalyst show the outstanding activity for photocatalytic hydrogen production under visible light (λ>420 nm). The composite photocatalyst with 3.0 wt.% $BiPO_4$ shows a optimum photocatalytic activity with H_2-production rate of 1110 μmol h^{-1} g^{-1}. The enhanced photocatalytic activity for P-C_3N_4 coupled with $BiPO_4$ comes from the high migration efficiency of photoinduced electrons on the interface of P-C_3N_4 and $BiPO_4$.

Keywords: Hydrogen production, Visible light, g-C_3N_4, $BiPO_4$, Heterostructured photocatalysts

Introduction

Polymeric graphitic carbon nitride (i.e. g-C_3N_4) materials have attracted much attention in recent years because of their interesting electronic properties and promising catalytic activities.[1] Considering the high thermal and chemical stabilities together with its semiconductor properties and low cost of mass production, g-C_3N_4 based materials are potentially close to anideal candidate for sustainable solar energy conversion systems.[2] With a narrow band gap of 2.7 eV, this polymeric semiconductor has been extensively explored as an attractive photocatalysis for the hydrogen roduction via solar photocatalytic water splitting.[3] Although the carbon nitrides have great applied potentials, the photocatalytic activity of pristine g-C_3N_4 is still deficient and the apparent quantum efficiency is only 1.5 %. With this in mind, it is one of fundamental interest to further promote the photocatalysis performance of such material sunder visible light irradiation.

To overcome this problem and enhance the photocatalytic performance of the carbon nitride system, a series of research strategies have been developed, including i) design and synthesis of favourable nanostructures of g-C_3N_4 such as nanoporous structures[4] and low-dimension nano architectures (e.g. nanorods[5], nanotubes[6] and nanosheets[7]), and ii) resorting to heterostructure modification of g-C_3N_4 such as chemical element doping (e.g. Boron[8], Iron[9] and Sulfur[10]) and synergistic component coupling (e.g. TiO_2[11], graphene[12] and Ag_3PO_4 [13]). First of all, the well-defined nanostructured materials especially allow for enhancing the efficiency of energy conversion by increasing the material surface area and shorting the bulk-to-surface distances. Furthermore, heterostructured modification often improves the photocatalytic activity of photocatalysts, when the recombination of photogenerated electrons and holes is effectively decreased, thus increasing the quantum efficiency.

In this investigation, we demonstrate unique 3-D nanoporous g-C_3N_4 nanosheets endowed with heterostructured modification by the binary phosphorus doping and $BiPO_4$ coupling, as a new complex catalyst system for visible-light photocatalytic hydrogen production. The novel complex catalyst

system is designed on the basis of the following considerations: (i) The 3-D nanoporous structures of nanosheets will provide the maximum accessibility for active species to the catalysts to ensure an effective mass transfer of reactants and/or products.[14] (ii) Phosphorus-doped g-C_3N_4 has showed remarkably enhanced photocurrent since the anticipated change of electronic structure for the g-C_3N_4.[15] (iii) The new type of $BiPO_4$ oxyacidsalt proved a high photocatalytic activity photocatalyst with high position of valence band and high separation efficiency of electron-hole pairs.[16] With these merits, we testify that visible-light photocatalytic hydrogen production with high efficiency can be designed on the basis of this hybrid nanomaterial.

Experimental

Materials Synthesis

In a typical hydrothermal synthesis progress, 20 mL amino cyanide (CH_2N_2) solution (50 wt.% in H_2O) was mixed with a certain quality of sodium di-hydrogen phosphate (NaH_2PO_4) in the presence of 20 mL diluted nitric acid solution, the mixed solution was ultrasound for 30 min and then transferred into a 50 ml Teflon-lined stainless steel autoclave and kept at 483 K for 4 h in an oven. After the autoclave was cooled down to room temperature, the sample was collected and calcined at 823 K for 4 h to obtain the finally phosphorus doping 3-D nanoporous graphene-like C_3N_4 nanosheets (P-C_3N_4). For the synthesis of $BiPO_4$ coupling 3-D nanoporous g-C_3N_4 nanosheets (P-C_3N_4/$BiPO_4$), bismuth nitrate ($Bi(NO_3)_3$•$5H_2O$) was a forehand dissolved into the diluted nitric acid solution without other procedures changed. An estimate of the $BiPO_4$ content in the nanoporous P-C_3N_4 nanosheets were obtained by changing the amounts of NaH_2PO_4 and $Bi(NO_3)_3$•$5H_2O$. For example, the P-C_3N_4/$BiPO_4$-1, indicated that 1 wt.% $BiPO_4$ has been coupled with P-C_3N_4 nanosheets.

Materials Characterization

The surface morphologies of the as-prepared samples were observed by thermal field emission environment scanning electron microscopy (FE-SEM, FEI, Quanta 400), and transmission electron microscopy (TEM, JEM-2010HR). The compositions and structures of the products were analyzed by X-ray diffraction (XRD, D8 ADVANCE X-ray diffractometer, CuKa radiation l=0.15418 nm) with a scanning rate of 10° min^{-1} in the 2-theta range from 10° to 70°. A Shimadzu spectrophotometer (model 2501 PC) equipped with an integrating sphere was used to record the UV-vis diffuse reflectance spectra of the samples. The X-ray photoelectron spectroscopy (XPS) was performed with a VG ESCALAB250 surface analysis system using a monochromatized Al KαX-ray source (300 W, 5 mA, and 15 kV). The BET-specific surface areas were measured by N_2 adsorption at liquid N_2 temperature in an ASAP 2010 analyser.

Photocatalytic experiments

Photocatalytic water splitting was carried out in a LabSolar H_2 photocatalytic hydrogen evolution system (Perfectlight, Beijing) including a 300 W Xe lamp (PLS-SXE300, Beijing Trusttech). In a typical reaction, 50 mg of the as-prepared samples was dispersed in a Pyrex glass reactor containing 100 mL of Na_2S (0.1 M) solution. Then the system was sealed and vacuumized to keep the pressure as-0.1 MPa. Afterwards, a circular cooling water system was turned on and the reactor was irradiated with Xe lamp (300 W) under magnetic stirring. The gases evolved were analyzed on line with a gas chromatograph (GC-7900, TCD, with N_2 as carrier gas) after 1 h of illumination. The reaction was continued for 5 h.

Results and discussion

The XPS result gives preliminary evidence of a P heteroatom in the modified g-C_3N_4 nanosheets as well as the degree of doping (Fig. 1), which is similar to that of previously reported P-doped carbon nitride solid (P possibly replace C position)[15]. The averaged content of phosphate was estimated to be

about 0, 0.85 and 1.7% with the increase of P-doped samples from pure g-C_3N_4 to P-C_3N_4 and P-C_3N_4/$BiPO_4$. Particularly, when it comes to P-C_3N_4/$BiPO_4$ (3 wt.%), the binding energy exhibits a positive one as compared to the P-C_3N_4 (131.6 vs 131.5 eV), these results show that the interaction between $BiPO_4$, P and g-C_3N_4 are not simply physical adsorption[16,17]. The XPS result indicates that the C/N ratio of pure-C_3N_4, P-C_3N_4 and P-C_3N_4/$BiPO_4$ (3 wt.%) is 0.782, 0.781 and 0.778, respectively, which is close to the expected value (0.750) of the theoretically predicted C_3N_4 empirical stoichiometry. This result further suggests that P possibly replace C position in the heterostructured modified g-C_3N_4 samples as reported by literature[15].

The microstructures of P-C_3N_4 nanosheets were first investigated by TEM. The TEM image reveals that the spatially 3-D P-C_3N_4 were stacked up by 2-D nanosheets layer by layer in three or more layers (Fig. 2 (A)). From the edges of P-C_3N_4 nanosheets, it is clearly to see the smooth surface, mesoporous structure and a rolling up edges, which clearly showed that the thickness of single P-C_3N_4 layer was about 30 nm (Fig. 2 (B)). The SEM images of phosphorus doped graphene like carbon nitride samples were further presented in Fig. 3. It can be seen that the P-C_3N_4 are pages-like overlapped by means of larger integrated nanosheets and well associated assembled by smaller fractured nanosheets from a front (Fig. 3 (A)) and aside view (Fig. 3 (B)), respectively. The flat surface and porous structure of nanosheets were more clearly identified from the high-magnification SEM images (Fig. 3 (C) and (D)). Specially, it is interesting that the space gaps between layers hinting at the confined sites may gave chance to those nano-sized species, such as nanorods and nanoparticles, grow in or out directly. We can grandly call these space gaps as “growth sits”. Furthermore, nitrogen adsorption-desorption measurement (see Fig. S1) show that the BET surface areas and total pore volumes of the porous g-C_3N_4 nanosheets were 45.72 m^2 g^{-1} and 0.183 cm^3 g^{-1}, respectively. The pore size distribution (inset of Fig. S1) indicates that the sample has a satisfactory nanoporous texture (10~150 nm).

Fig. 4 shows the contrastive TEM images of P-C_3N_4 and P-C_3N_4/$BiPO_4$ (3 wt.%) samples. The TEM images of P-C_3N_4 clearly show a hierarchical and inter-connected 3-D nanoporous architecture and the pore size is in the range from 10 to 100 nm (Fig. 4 (A) and (B)). On the other hand, well-defined and fairly long nanorods, whose average diameter is about 200 nm and whose surface is distinctly enwrapped with smooth, flayers and gauze-like P-C_3N_4 nanosheets, could be obtained in the cases of P-C_3N_4/$BiPO_4$ nanocomposites (Fig. 4 (C)). The results well indicated that $BiPO_4$ nanorods were distributed into P-C_3N_4 nanosheets in the composite samples, there are no apparent aggregation of $BiPO_4$ which means the formation of interfaces between $BiPO_4$ and P-C_3N_4. It is also observed that the P-C_3N_4 still has the mesoporous nanosheets structure after coupling with $BiPO_4$ nanorods. Fig. 4(D) shows the HRTEM images of the interfaces between $BiPO_4$ nanorods and P-C_3N_4 nanosheets. From the HRTEM images we can infer: (i) on the basis of the lattice spacing of 0.303 nm was correspond to the (200) planes of $BiPO_4$ (shown in Fig. S2), indicating that the nanorods in Fig. 4(C) were exactly $BiPO_4$ nanorods. (ii) the existence of some $BiPO_4$ nanorods were between P-C_3N_4 layers, apparently, the bright portions (in the yellow line) were attributed to the pore of P-C_3N_4 nanosheets and the dark parts on $BiPO_4$ nanorods were refer to the existence of P-C_3N_4, all these demonstrate that there are at least one layer of P-C_3N_4 nanosheet covered on the surface of $BiPO_4$ nanorods. (iii) the natural existed of "growth sits" on 3-D porous nanosheets architectural structure, which may efficient avoid strongly aggregation of $BiPO_4$ nanorods during the synthesised process. The TEM image of comparing experiment pure $BiPO_4$ nanorods was showed in Fig. S3, whose length (about 600 nm) is much shorter than that in P-C_3N_4/$BiPO_4$ (about 2000 nm). Taken together, a novel sandwich-like heterocrystals have been obtained by a simple one-step hydrothermal synthesis progress. In addition, as the lattice and energy level between C_3N_4 and $BiPO_4$ is match well, the heterojunctions could promote the transfer and separation of photoexcited electron-hole pares under visible light irradiation.

The XRD pattern of P-C_3N_4 nanosheets and P-C_3N_4/$BiPO_4$ composited photocatalysts were shown in Fig. 5(A). From XRD pattern, two peaks at around 13° and 27.4° of P-C_3N_4 were corresponding to in-plane structural packing motif of tri-s-triazine which is indexed as (100) peak and interlayer graphitic packing motif of aromatic segments which is indexed as the (002) peak for graphitic materials[1], respectively. These two feature diffraction peaks of g-C_3N_4 suggest that the original atomic structure is largely retained, which the evidence is denoted as graphitic 3-D P-C_3N_4 with layer by layer structure. The P-C_3N_4/$BiPO_4$ samples with different proportion (defined as $BiPO_4$: P-C_3N_4 wt.% discriminated by the mass of initial reaction precursors) were synthesized. The diffraction peaks of P-C_3N_4/$BiPO_4$ compounds clearly revealed the cubic phase of $BiPO_4$ (JCPDS No: 15-0766) and crystalline P-C_3N_4 peak. All the P-C_3N_4/$BiPO_4$ samples exhibit diffraction peaks corresponding to both g-C_3N_4 and $BiPO_4$, and no other impure peaks can be observed, suggesting a two-phase composition of g-C_3N_4 and $BiPO_4$ in these composites. Combining with TEM analysis the two-phase materials connected so closely that they advantageously formed heterojunction structure which is proved that could decrease the recombination rate of photogenerated electrons and holes, and contribute to promote the utilization efficiency of photo-generated electrons.[18] As we all know, the improvement in mobility of the charge is important to photocatalysts. Fig. 5(B) shows the result of UV-visible diffuse reflectance (DRS) spectra of P-C_3N_4 and P-C_3N_4/$BiPO_4$ composited photocatalysts. It has been reported that the absorption edge of the pure $BiPO_4$ occurred at about 330 nm.[19, 20] However, when $BiPO_4$ loaded on the inter-surface of 3-D P-C_3N_4 nanosheets, the ability of light absorption was enhanced in all of the wavelength range from 200 to 700 nm. Interestingly, it is also found that the absorption of the P-C_3N_4/$BiPO_4$ composites increased upon the addition of $BiPO_4$ nanorods. These results may be attributed to two major reasons. First of all, the interaction of heterojunction between $BiPO_4$ and P-C_3N_4 effectively accelerates the separation of electron-hole pairs account for the band-gap transition of photo-generated electrons, and then enhanced the absorption in

the visible-light region. Secondly, as a colour change of the composites samples, which become darker, that is, from pale yellow to grey, along with a higher amount of $BiPO_4$ was introduced into the 3-D P-C_3N_4 nanosheets would also cause the absorbance enhanced.

It has been investigated that $BiPO_4$ possesses a wide band gap which limits its photo-absorption to only the UV region, normally accounting for ca. 5% of the total sunlight, which is undoubtedly important to develop photocatalytic materials that harvest a wide range of visible photons.[20] In addition, there are few research has applied bismuth phosphate as a photocatalyst using in water splitting for producing hydrogen. In this study, the $BiPO_4$ nanorods were successfully growing in the inter space of 3-D mesoporous P-C_3N_4 nanosheets, and the novel 3-D structure composited photocatalysts were first detected the performance of visible light photocatalytic activity in direct water splitting into H_2.

Fig 6 (A) shows a standard curve obtained by plotting the peak area, which was detected by a Labsolar H_2 photocatalytic hydrogen evolution system (Perfect light, Beijing) with gas chromatography (GC-14C, Shimadzu, Japan, TCD), against the known number of hydrogen counts, such as 0, 100, 200, 300, 400, 500 μmol per tube. The line has a slope of 9.015×10^{-4} and corresponding coefficient of determination R^2 of 0.998. As the curve was passing through the origin point, the H_2 content can be calculated as the following standard equation:

$$Y_{H2}(\mu mol) = 0+b\bullet X = 9.015\times10^{-4}\bullet X \text{ (peak area)}$$

Here, we take P-C_3N_4/$BiPO_4$ (3 wt.%) as a concrete case to experiment the hydrogen gas producing by irradiating with visible light during the five hours. Fig. 6(B) gave out the actual hydrogen gas testing chart detected by gas chromatography. The exact location of the detected hydrogen peaks was consistent at time of 1.23 min and the peak areas were gradually increased with the time prolonged. This measured experimental results also demonstrated the stability of the testing system. Fig. 6(C) presents a comparison of the pure 3-D P-C_3N_4 and all the synthesised $BiPO_4$ coupling samples. As can

be seen from this figure, the $BiPO_4$ content has a significant influence on the photocatalytic activity of P-C_3N_4 and all the samples exhibit very stable activity during the 5-h irradiation. Obviously, the amount of H_2 production over P-C_3N_4/$BiPO_4$ (3 wt.%) was much more than that of the other samples. From Fig. 6 (D), it can be seen that the H_2 production rate of P-C_3N_4 sample was 676 μmol h^{-1} g^{-1}, however, when the content of $BiPO_4$ was increased to 3 wt.%, the H_2 production rate reached the highest value of 1110 μmol h^{-1} g^{-1}. In this regard, the photocatalytic activity of sample P-C_3N_4/$BiPO_4$ (3 wt.%) exceeds that of pure P-C_3N_4 by a factor of 1.64, and the H_2-production rate is significantly greater than that of most C_3N_4-basis semiconductor photocatalysts. The present results also showing that a suitable loading content of grapheme is crucial for optimizing the photocatalytic activity of P-C_3N_4/$BiPO_4$ 3-D nanocomposits.

In corresponding experiment, no hydrogen was detected when $BiPO_4$ nanorods were used as the photocatalyst with Pt as a cocatalyst under visible light irradiation, suggesting that the bare $BiPO_4$ without P-C_3N_4 nanosheets is likely not active for photocatalytic H_2 production under the experimental conditions studied (shown in Fig. 6 (C) and (D)). On the basis of the above results, a photocatalytic mechanism of the P-C_3N_4/$BiPO_4$ under visible-light irradiation can be proposed (Fig. 7). Under visible-light irradiation, electrons (e^-) are excited from the valence band (VB) to the conduction band (CB) and created holes (h^+) in the VB. Normally, for pure P-C_3N_4, the charges are likely transfer in one of three following ways: (i) injected to Pt nanoparticles located on the P-C_3N_4 nanosheets; (ii) directly onto the surface of P-C_3N_4 nanosheets; (iii) quickly recombine with the h^+ one the VB. The accumulated e^- on the Pt and the CB of P-C_3N_4 can effectively reduce H_2O (or H^+) to produce H_2, while holes at the VB of P-C_3N_4 accumulated and can react with methanol as a sacrificial reagent. Once $BiPO_4$ was introduced to the P-C_3N_4 nanosheets, as the reported previously, the highest occupied molecular orbital (HOMO) of g-C_3N_4 was more negative than the conduction band of $BiPO_4$ (-1.12 V vs -0.65 V)[3, 21] the photo-generated charge on P-C_3N_4 can directly transfer to the CB of

$BiPO_4$ (occurred step (i) or (ii)), eventually the electrons react with the adsorbed H^+ ions to form H_2, and reducing the probability of electron-hole recombination and resulting in an enhanced photocatalytic activity which driven by band potentials between two semiconductors. Furthermore, the interaction of heterojunction between $BiPO_4$ and P-C_3N_4 effectively accelerated the charge transfer the two semiconductor would be more spatially smooth, which is fundamental for the improvement of photocatalytic activity. The unique 3-D structure of P-C_3N_4/$BiPO_4$ allowed the photocatalytic reactions to take place not only on the surface of semiconductor catalysts, but also on the inset space between the layers of P-C_3N_4 nanosheets, effectively increasing the reaction sites.

Conclusions

In this work, we demonstrate unique 3-D nanoporous g-C_3N_4 nanosheets endowed with heterostructured modification by the binary phosphorus doping and $BiPO_4$ coupling, as a new complex catalyst system for visible-light photocatalytic hydrogen production. Results show that pure $BiPO_4$ could not split water directly under visible light irradiation. However, comparing the energy levels of C_3N_4 with $BiPO_4$, it is fortunate to notice that their well-matched overlapping band-structures are quite suitable to construct heterostructures that would bring an effective separation and transfer of photogenerated charges, which would remarkable, enhance the visible-light photocatalytic H_2-production activity of the composited semiconductors. The optimal $BiPO_4$ content was found to be 3.0 wt.%, and the corresponding H_2-production rate was 1110 μmol h^{-1} g^{-1}. The unique 3-D mesoporous structure of P-C_3N_4 nanosheets effectively increasing the reaction sites to allow the photocatalytic reactions to take place. Those may be an expected opportunity for g-C_3N_4 on element doping and other inorganic semiconductor modification by the novelty one-step hydrothermal synthesis progress.

Acknowledgements

This research was supported by NSF of China (21105030 and 21173088) and the key Academic Program of the 3rd phase ‘‘211 Project’’ of South China Agricultural University. The authors thank the Foundation for High-level Talents in Higher Education of Guangdong Province and Guangdong Natural Science Foundation (S2013040013755), Colleges and Universities in Guangdong Province Science and Technology Innovation Project (2013KJCX0123). Special thanks to Prof. Can Li in State Key Laboratory of Catalysis, Dalian Institute of Chemical Physics, Chinese Academy of Sciences. This work also partly supported by the State Key Laboratory of Catalysis cooperation project (N-08-08).

Notes and references

1. J. Xu, L. Zhang, R. Shia, Y. Zhu, *J. Mater. Chem.* A, 2013, **1**, 14766-14772.
2. J. Low, S. Cao, J. Yu, S. Wageh, *Chem. Commun.*, 2014, DOI: 10.1039/C4CC02553A.
3. X. Wang, K. Maeda, A. Thomas, K. Takanabe, G. Xin, J. M. Carlsson, K. Domen and M. Antonietti, *Nat. Mater.*, 2009, **8**, 76-80.
4. S. Yang, W. Zhou, C. Ge, X. Liu, Y. Fang, Z. Li, *RSC Adv.*, 2013, **3**, 5631-5638.
5. X.-H. Li, J. Zhang, X. Chen, A. Fischer, A. Thomas, M. Antonietti and X. Wang, *Chemistry of Materials*, 2011, **23**, 4344-4348.
6. J. Gao, Y. Zhou, Z. Li, S. Yan, N. Wang, Z. Zou, *Nanoscale*, 2012, **4**, 3687-3692
7. L. Lin, Z. Cong, J. Li, K. Ke, S. Guo, H. Yang, *J. Mater. Chem. B*, 2014, **2**, 1031-1037.
8. S. C. Yan, Z. S. Li and Z. G. Zou, *Langmuir*, 2010, **26**, 3894-3901.
9. X. Chen, J. Zhang, X. Fu, M. Antonietti and X. Wang, *J. Am. Chem. Soc.*, 2009, **131**, 11658-11659.
10. J. Zhang, J. Sun, K. Maeda, K. Domen, P. Liu, M. Antonietti, X. Fu and X. Wang, *Energ. Environ. Sci.*, 2011, **4**, 675.
11. Y. Zang, L. Li, Y. Xu, Y. Zuo, G. Li, *J. Mater. Chem. A*, 2014, DOI: 10.1039/C4TA02082K.

12. K. Dai, L. Lu, Q. Liu, G. Zhu, X. Wei, J. Bai, L. Xuana, *Dalton Trans.,* 2014, **43**, 6295-6299.

13. S. Kumar, T. Surendar, A. Baruah, V. Shanke, *J. Mater. Chem. A,* 2013*,* **1***,* 5333-5340.

14. C. Hu, H. Cheng, Y. Zhao, Y. Hu, Y. Liu, L. Dai and L. Qu, *Adv. Mater.*, 2012, **24**, 5493-5498.

15. Y. Zhang, T. Mori, J. Ye, M. Antonietti, *J. Am. Chem. Soc.*, 2010, **132**, 6294-6295.

16. C. Pan, J. Xu, Y. Wang, D. Li and Y. Zhu, *Adv. Funct.l Mater.*, 2012, **22**, 1518-1524.

17. A. K.-V. Alexander V. Naumkin, Stephen W. Gaarenstroom, and Cedric J. Powell, *The U.S. Secretary of Commerce on behalf of the United States of America*, 2012, **http://srdata.nist.gov/xps/**.

18. L. Zhang, H. Cheng, R. Zong and Y. Zhu, *J. Phys. Chem. C*, 2009, **113**, 2368-2374.

19. C. Pan, D. Li, X. Ma, Y. Chen and Y. Zhu, *Catalysis Science & Technology*, 2011, **1**, 1399.

20. Z. Li, S. Yang, J. Zhou, D. Li, X. Zhou, C. Ge, Y. Fang, *Chem. Eng. J.*, 2014, **241**, 344-351.

21. C. Pan and Y. Zhu, *Environmental Science & Technology*, 2010, **44**, 5570-5574.

Figure captions

Fig. 1 (A) XPS spectrum of phosphors recorded from pristine surface of pure-C_3N_4, P-C_3N_4 and P-C_3N_4/$BiPO_4$ 3 wt.%, and (B) molecule structure model of P-C_3N_4 constitution unit.

Fig. 2 Typical TEM images of P-C_3N_4 nanosheets in different magnification.

Fig. 3 Typical SEM image of the P-C_3N_4 nanosheets from different viewpoints. (A) front and (B) side, (C) and (D) High-magnification image from (A) and (B) .

Fig. 4 Contrastive TEM images of the P-C_3N_4 (A, B) and P-C_3N_4/$BiPO_4$ 3 wt.% (C, D) samples.

Fig. 5 (A) XRD pattern and (B) UV-vis diffuse-reflectance spectra of all the synthesised samples. a: Pure mpg P-C_3N_4, b: P-C_3N_4/$BiPO_4$-1, c: P-C_3N_4/$BiPO_4$-3, d: P-C_3N_4/$BiPO_4$-5, e: P-C_3N_4/$BiPO_4$-7.

Fig. 6 (A) Standard curve for the quantitative estimation of hydrogen gas; (B) the actual hydrogen gas testing chart detected by gas chromatography; (C) the time course of H_2 evolution under visible irradiation over all the synthesised samples; (D) Comparison of the visible-light photocatalytic activity of samples for H_2 production using 10% methanol aqueous solution as a sacrificial reagent and 0.3 wt.% Pt as a co-catalyst; Light source: Xe lamp (300 W) with an optical filter (λ> 420 nm). a: Pure mpg P-C_3N_4, b: P-C_3N_4/$BiPO_4$-1, c: P-C_3N_4/$BiPO_4$-3, d: P-C_3N_4/$BiPO_4$-5, e: P-C_3N_4/$BiPO_4$-7, f: pure-$BiPO_4$.

Fig. 7 Schematic illustration of the charge separation and transformationin the P-C_3N_4 nanosheets-$BiPO_4$ nanorods system under visible light irradiation.

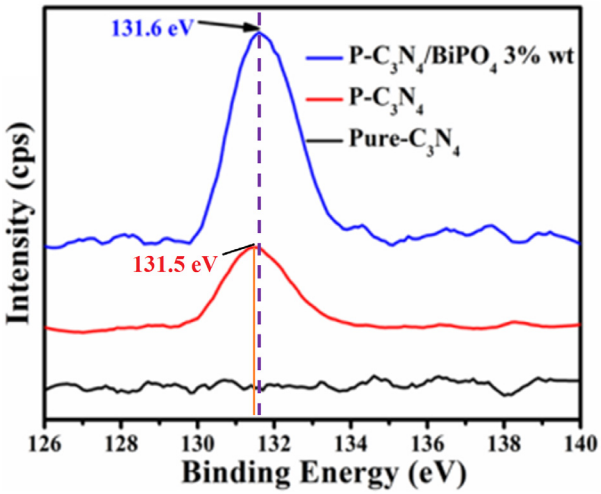

Fig. 1 (A) XPS spectrum of phosphors recorded from pristine surface of pure-C_3N_4, P-C_3N_4 and P-C_3N_4/$BiPO_4$ 3 wt.%, and (B) molecule structure model of P-C_3N_4 constitution unit.

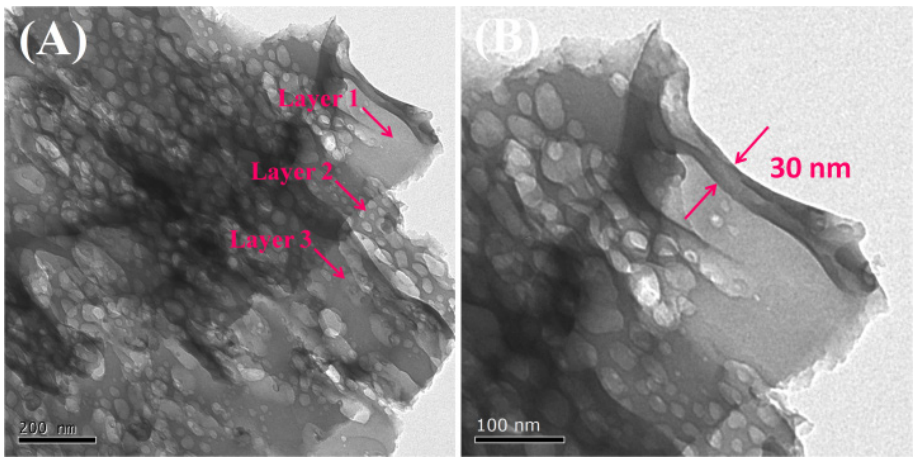

Fig. 2 Typical TEM images of P-C_3N_4 nanosheets in different magnification.

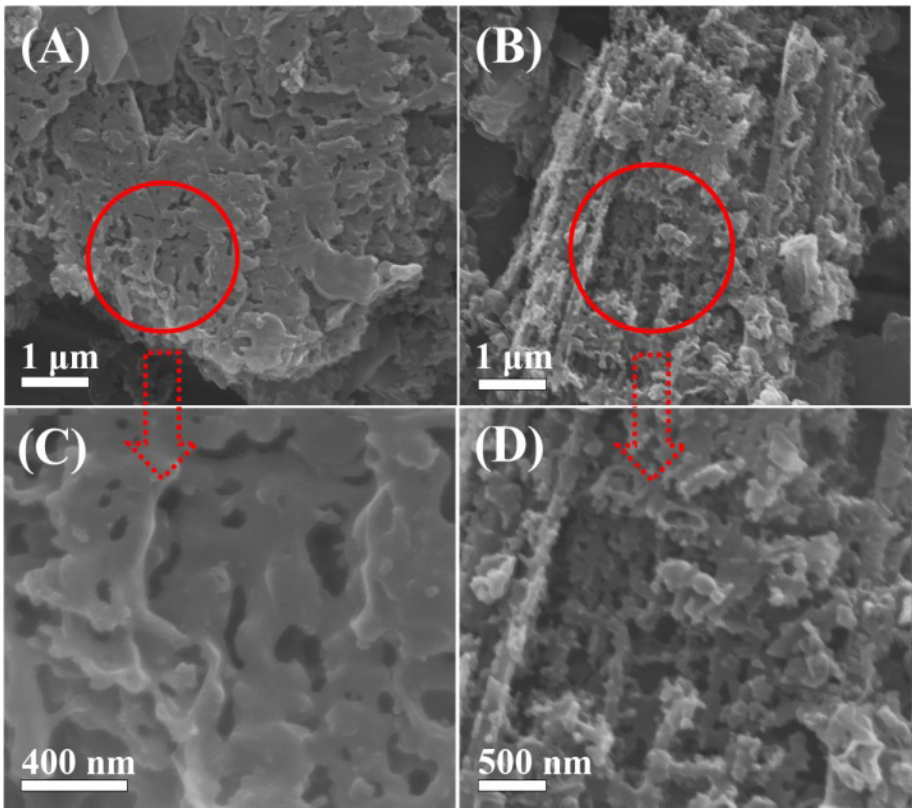

Fig. 3 Typical SEM image of the P-C_3N_4 nanosheets from different viewpoints. (A) front and (B) side, (C) and (D) High-magnification image from (A) and (B) .

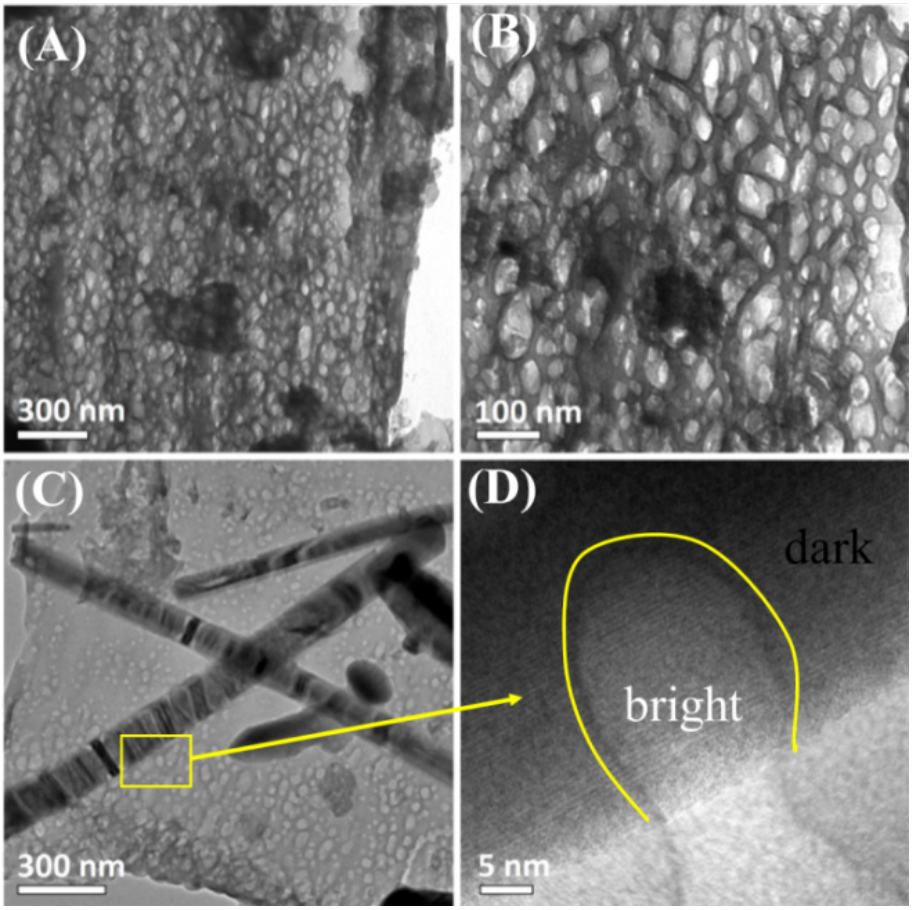

Fig. 4 Contrastive TEM images of the P-C_3N_4 (A, B) and P-C_3N_4/$BiPO_4$ 3 wt.% (C, D) samples.

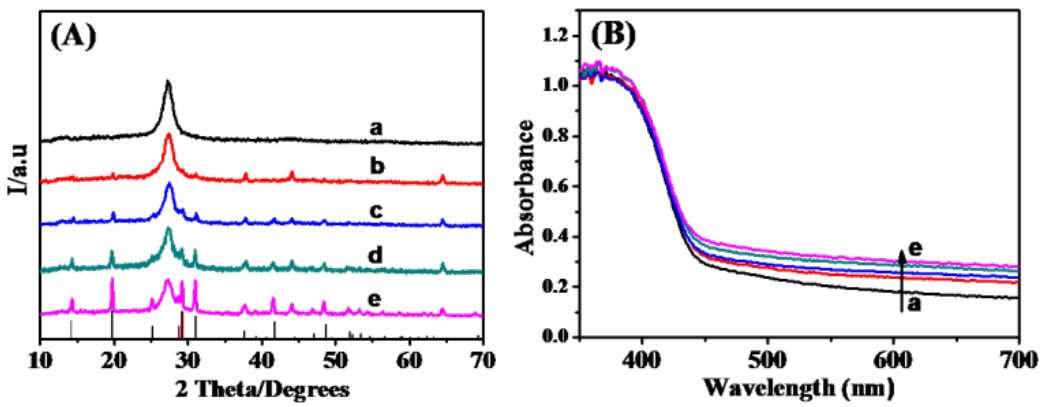

Fig. 5 (A) XRD pattern and (B) UV-vis diffuse-reflectance spectra of all the synthesised samples. a: Pure mpg P-C_3N_4, b: P-C_3N_4/$BiPO_4$-1, c: P-C_3N_4/$BiPO_4$-3, d: P-C_3N_4/$BiPO_4$-5, e: P-C_3N_4/$BiPO_4$-7.

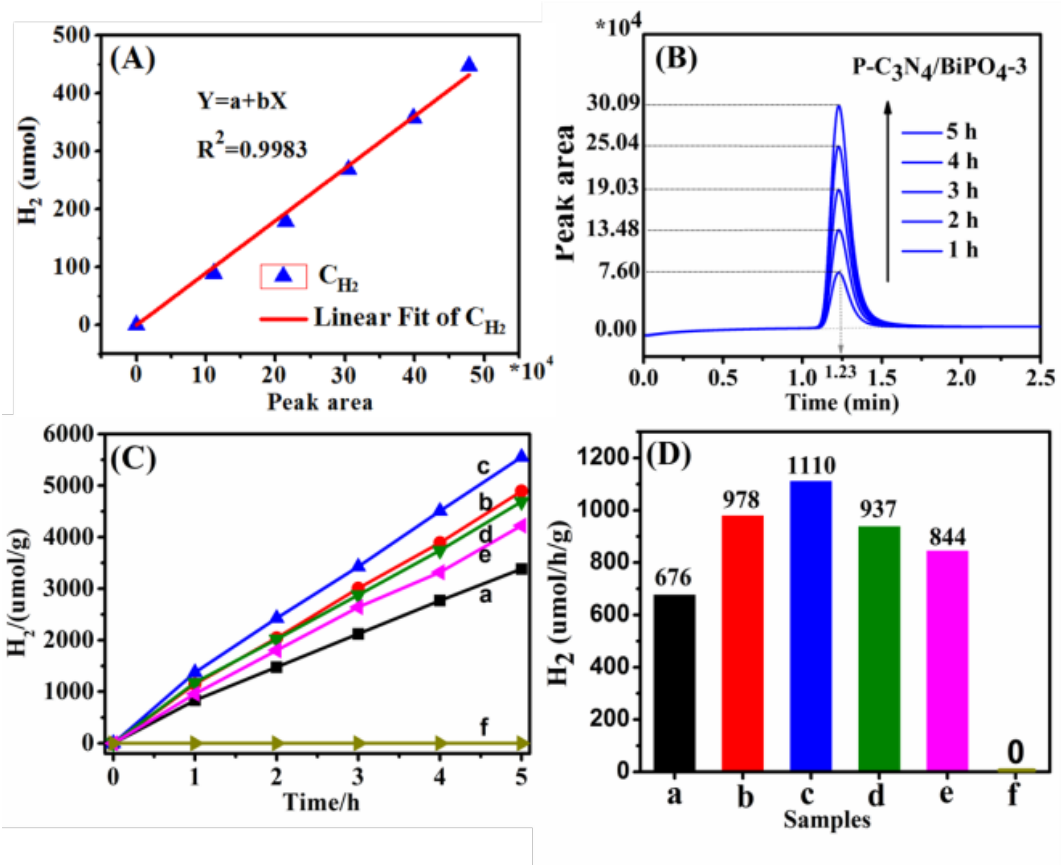

Fig. 6 (A) Standard curve for the quantitative estimation of hydrogen gas; (B) the actual hydrogen gas testing chart detected by gas chromatography; (C) the time course of H_2 evolution under visible irradiation over all the synthesised samples; (D) Comparison of the visible-light photocatalytic activity of samples for H_2 production using 10% methanol aqueous solution as a sacrificial reagent and 0.3 wt.% Pt as a co-catalyst; Light source: Xe lamp (300 W) with an optical filter (λ> 420 nm). a: Pure mpg P-C_3N_4, b: P-C_3N_4/$BiPO_4$-1, c: P-C_3N_4/$BiPO_4$-3, d: P-C_3N_4/$BiPO_4$-5, e: P-C_3N_4/$BiPO_4$-7, f: pure-$BiPO_4$.

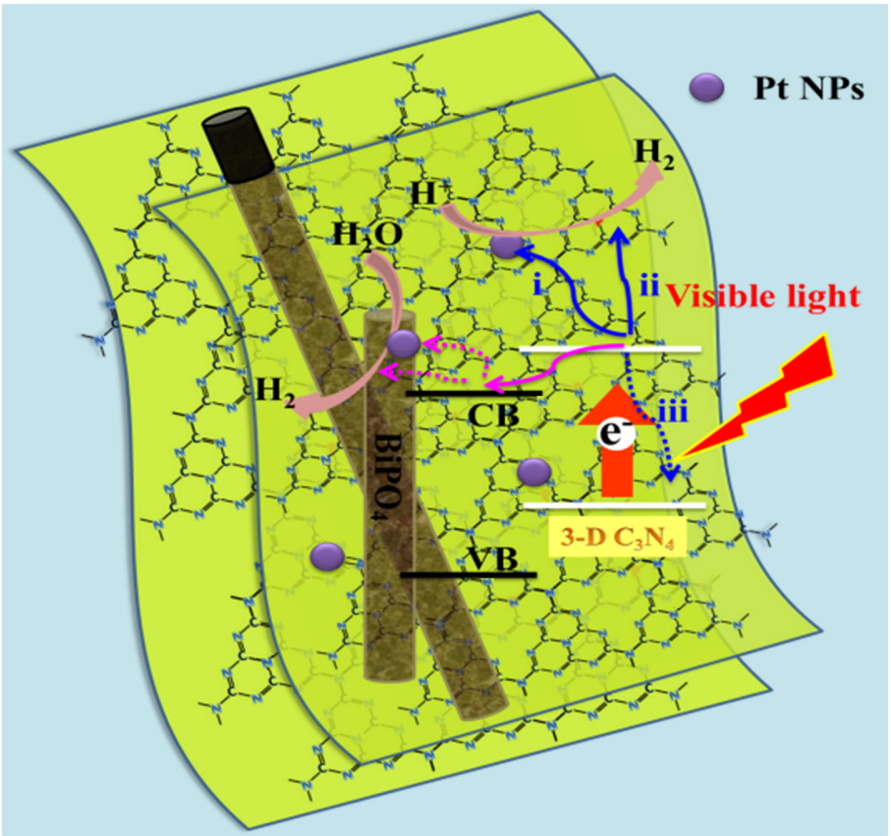

Fig. 7 Schematic illustration of the charge separation and transformationin the P-C_3N_4 nanosheets-$BiPO_4$ nanorods system under visible light irradiation.

5